ELSEVIER

Contents lists available at ScienceDirect

# Chemical Physics Letters

journal homepage: www.elsevier.com/locate/cplett





# Characterization of the intermolecular vibrational levels bound within the $Ar+I_2(E,\,v)$ potential energy surfaces

Camille Makarem<sup>1</sup>, Richard A. Loomis

Department of Chemistry and Institute of Materials Science and Engineering, Washington University in St. Louis, St. Louis, MO 63130, USA

ABSTRACT

Two-color, two-photon laser-induced fluorescence experiments were performed to probe the intermolecular interactions within the Ar +  $I_2(E, v_E = 0-3)$  potential energy surfaces. Spectra were recorded using the lowest-energy T-shaped level and an excited intermolecular vibrational level with bending excitation within the Ar +  $I_2(B, v_B = 23)$  potential as intermediate levels to guide the spectral assignments. Progressions of intermolecular stretching and bending levels bound within the Ar +  $I_2(E, v_E)$  potentials were identified, and their vibrational frequencies were determined. The harmonic frequency and anharmonic constant for the bending vibrational mode were determined to be  $\omega_e(b) \sim 34.8 \text{ cm}^{-1}$  and  $\omega_e\chi_e(b) \sim 0.3 \text{ cm}^{-1}$ . The frequency and anharmonic constant for the stretching mode were found to be the same as reported previously [V.V. Baturo, et al. Chem. Phys. Lett. 647 (2016) 161],  $\omega_e(s) = 37.2(1.1) \text{ cm}^{-1}$  and  $\omega_e\chi_e(s) = 1.8(2) \text{ cm}^{-1}$ .

#### 1. Introduction

The Ar···I $_2$  complex has proven to be a model system for investigating long-range intermolecular interactions and energy-transfer processes [1–4]. Much of the work on this system has focused on characterizing the interactions within the Ar + I $_2$  potential energy surfaces (PESs) associated with the I $_2$  B( $^3\Pi_{0u}^+$ ) excited-electronic state and to a lesser degree the I $_2$  X( $^1\Sigma_0^+$ ) ground-electronic state [3–11]. Numerous fluorescence-based spectroscopy experiments [9–13] as well as high-level calculations [6,14,15] determined there are two distinct conformers bound within the ground-state PES, a T-shaped Ar···I $_2$ (X, v $_X$  = 0) conformer with the Ar atom localized equidistant from each I atom and a linear conformer with the Ar atom localized at either end of the I–I molecular axis. The linear conformer is more energetically stable than the T-shaped conformer, with binding energies of 250.3(2.7) and 240.5 (3.6) cm $^{-1}$ , respectively [9,12,16].

Features associated with transitions of both conformers were identified in excitation spectra of Ar···I<sub>2</sub> clusters stabilized in a supersonic expansion and recorded throughout and above the I<sub>2</sub> B–X, v<sub>B</sub>–0 spectral region [9–13]. The Ar + I<sub>2</sub>(B, v<sub>B</sub>) excited-state PESs have a minimum in the T-shaped geometry, and the lowest-lying intermolecular vibrational levels localized in this region are accessible via transitions of the ground-state T-shaped Ar···I<sub>2</sub>(X, v<sub>X</sub> = 0) conformer [6,9,17,18]. Since the binding energy of the B-state complex is slightly less than that of the ground-state T-shaped conformer [9,16], these transitions result in vibronic spectra that contain a progression of features that start just

above and extend to higher transition energies than each  $I_2$  B–X,  $v_B$ –0 monomer band [1,5,8–10]. Transitions of the ground-state linear Ar···I $_2$ (X,  $v_X$  = 0) complex access higher-lying intermolecular vibrational levels, many of which are delocalized in the angular coordinate, representing motion of the Ar atom about the I–I moiety, thereby sampling a wide range of intermolecular orientations, including the linear geometry [6,0]

Far less information is known about the intermolecular interactions of Ar...I2 within the PESs associated with the ion-pair states of I2 [19-22]. Experiments performed using two-color, two-photon laserinduced fluorescence (LIF) spectroscopy accessed the intermolecular vibrational levels within the Ar +  $I_2(E, v_E = 0-4)$  PESs [19,20]. In those experiments, the ground-state T-shaped Ar $\cdots$ I<sub>2</sub>(X, v<sub>X</sub> = 0) conformer was promoted to the lowest-energy T-shaped Ar $\cdots$ I<sub>2</sub>(B,  $v_B = 19$ , n' = 0) intermediate level with  $E_1 = 17814.4 \text{ cm}^{-1}$ . The label n' indicates the energetic ordering of the intermolecular levels bound within each Ar +  $I_2(B, v_B = 19)$  PES [9]. The pulses of a second laser were overlapped in time with the first, and the wavenumber of this laser,  $E_2$ , was scanned through the  $I_2$  E-B,  $v_E$ -19 spectral region to access the Ar $\cdots$ I<sub>2</sub> intermolecular vibrational levels bound within the Ar + I<sub>2</sub>(E,  $v_E$ ) PESs. The fluorescence from I2 dissociation product molecules formed in the ionpairs states was then monitored as a function of  $E_2$ . Progressions of Ar...I<sub>2</sub> spectral features attributed to intermolecular stretching levels were identified in these two-photon LIF spectra, and no features were associated with intermolecular bending levels. Some of the spectral congestion was associated with several spectral components present in

E-mail address: loomis@wustl.edu (R.A. Loomis).

<sup>\*</sup> Corresponding author.

<sup>&</sup>lt;sup>1</sup> Present address: Laser Interferometer Gravitational-Wave Observatory (LIGO) Laboratory, California Institute of Technology, Pasadena, CA 91125, USA

the  $E_2$  pulses [20]. Nevertheless, an intermolecular stretching frequency of  $\sim 38~{\rm cm}^{-1}$  was determined [20]. Baturo, et al [20] also determined a binding energy of the T-shaped complex in the Ar + I<sub>2</sub>(E, v<sub>E</sub> = 0–4) PESs to be in the range of 410.4(2) to 415.0(2) cm<sup>-1</sup>, with increasing binding energies with higher v<sub>E</sub>.

Theoretical results reported on the Ar + I<sub>2</sub>(E, v<sub>E</sub>) PESs are not particularly consistent with the experimental data reported thus far. Shcherbul', et al. [23,24] used a diatomics-in-molecule with first-order perturbation (IDIM PT1) method with multiple models to include additional interactions to characterize the Ar + I<sub>2</sub>(E, v<sub>E</sub>) intermolecular PES as well as those associated with other  $I_2$  ion-pair states. The overall minimum of the Ar + I<sub>2</sub>(E,  $v_E$ ) PES is in the T-shaped geometry with a calculated well depth as small as 204 cm<sup>-1</sup> or as large as 965 cm<sup>-1</sup>, depending on the interactions included [23,24]. Note the binding energy of the lowest-energy, T-shaped level in the Ar +  $I_2(E, v_E)$  PES is likely greater than in the Ar +  $I_2(X, v_X = 0)$  and Ar +  $I_2(B, v_B = 21)$  PESs, 240.5 and 227.2 cm<sup>-1</sup> [16], respectively, based on trends for other rare gas···dihalogen complexes [25,26]. The only intermolecular  $Ar + I_2$  PES for an ion-pair state with a minimum calculated for the linear orientation is the Ar +  $I_2(D', v_{D'})$  system; the calculated well depths for the linear geometry range from 123 to 579 cm<sup>-1</sup>, depending on the interactions included [23].

Questions regarding the details of the Ar +  $I_2(E,$   $v_E)$  PESs, the intermolecular vibrational levels bound within them, and the dynamics that result when complexes are prepared in those levels remain. For instance, why are spectral features associated with both intermolecular bending and stretching levels identified in two-color, two-photon LIF spectra of the more weakly bound He +  $I_2(E,$   $v_E)$ , He + ICl(E,  $v_E)$ , and He + ICl( $\beta$ ,  $v_\beta$ ) PESs [25,26], but not of the more strongly bound Ar +  $I_2(E,$   $v_E)$  potential? In this letter, we report on the results of two-color, two-photon LIF experiments aimed at further interrogating the properties of the Ar +  $I_2(E,$   $v_E)$  PESs. In contrast to the previous experiments [19,20], different intermediate levels were used to access contrasting Franck-Condon spectral windows to the Ar +  $I_2(E,$   $v_E)$  potential and identify intermolecular levels that span varying regions of the PES.

## 2. Experimental methods

Ground-state linear and T-shaped Ar $\cdots$ I<sub>2</sub>(X,  $v_X = 0$ ) complexes were stabilized in a pulsed, supersonic expansion, as previously described [4,9,16,27]. Unless otherwise stated, experiments were performed using a gas mixture comprised of 10% Ar in He and a backing pressure of  $\sim$ 7000 Torr that was passed over room-temperature iodine crystals and pulsed into vacuum. The third harmonic, 355 nm, of one nanosecond pulsed Nd:YAG laser was used to pump a tunable dye laser that accessed the  $I_2$  B-X,  $v_B$ -0 spectral region. This excitation laser, with wavenumber  $E_1$ , was fixed on the transition of the T-shaped Ar···I<sub>2</sub>(X,  $v_X = 0$ ) complex to either the lowest-energy intermolecular vibrational level, n'=0, which also has a rigid T-shaped geometry, or the n'=2, third-energy level, which has intermolecular bending excitation in the I<sub>2</sub> B-X, 23-0 spectral region [9,10,28]. The pulses of a second nanosecond dye-laser system, pumped by the 355-nm output of a second Nd:YAG laser, were counter propagated with the excitation-laser at a distance of 15 mm downstream from the pulsed valve. The timing between the pulses was digitally controlled, and most of the spectra were recorded with the  $E_1$ and  $E_2$  pulses overlapped in time in the region of the supersonic expansion. The two-color, two-photon LIF spectra were recorded by fixing  $E_1$  on a known Ar···I<sub>2</sub> transition in the I<sub>2</sub> B–X, 23–0 region and scanning the wavenumber of the second laser, E2, throughout the I2 E-B,  $v_{E}\!\!-\!\!23$  region, where  $v_{E}=0\!\!-\!\!3.$  The two lasers had pulse fluences of  $\sim15$ and 32-64 mJ cm $^{-2}$ , respectively, pulse durations of  $\sim$  5 ns, and bandwidths of  $\sim 0.03 \text{ cm}^{-1}$ . Fluorescence from the  $I_2$  ion-pair states was preferentially collected with an optical telescope assembly, a UG-11 glass filter, and a photomultiplier tube (PMT). The laser wavenumbers were calibrated using multiple spectrometers and by recording similar two-color, two-photon LIF spectra with E<sub>1</sub> fixed on specific I<sub>2</sub> B–X, v<sub>B</sub>–0

molecular transitions and scanning  $E_2$  across known  $I_2$  E–B,  $v_E$ – $v_B$  transitions [9,29].

#### 3. Results and discussion

A two-color, two-photon LIF spectrum recorded throughout most of the  $I_2$  E-B,  $v_E$ -23 ( $v_E$  = 0-3) spectral region is included in Fig. 1, top, black spectrum. This spectrum was obtained using the T-shaped,  $Ar \cdot I_2(B, v_B = 23, n' = 0)$  metastable level as the intermediate,  $E_1 =$ 18169.57 cm<sup>-1</sup>. This excitation spectrum is nearly identical to the spectra reported by Baturo, et al [19,20]; there is a slight difference in the overall intensity profiles of the spectra, but this is not surprising considering the laser-fluence profiles over the broad wavenumber region spanned by the spectra were likely dissimilar in the different experiments. In order to differentiate those LIF features associated with transitions from the short-lived Ar···I<sub>2</sub>(B,  $v_B = 23$ , n') intermediate levels, ~50 ps [10], from  $I_2$  E–B,  $v_E$ – $v_B$  or  $\beta$ –B,  $v_\theta$ – $v_B$  transitions [29,30] of  $I_2(B,\,v_B < 23)$  dissociation products, spectra were also collected with the  $E_2$  scanning laser pulses delayed by 20 ns from the  $E_1$  fixed-energy, excitation pulses. Only features associated with transitions of the longlived I<sub>2</sub>(B, v<sub>B</sub>) products are observed in these spectra, red, middle spectrum in Fig. 1. These  $I_2$   $\beta$ –B,  $v_{\beta}$ – $v_B$  spectral assignments were further verified by recording I<sub>2</sub> spectra in this region. For example, the inverted, grey spectrum at the bottom of Fig. 1 was recorded with  $E_1$  fixed on the maximum of the  $I_2$  B–X, 20–0 monomer transition,  $E_1 = 17892.88$  cm<sup>-1</sup>, and with  $E_2$  delayed by 20 ns from  $E_1$ . The Ar +  $I_2$ (B,  $v_B = 20$ ) product channel is the highest-energy product channel for excitation of the  $Ar \cdot I_2(B, v_B = 23, n' = 0)$  complexes [4]. The features labeled with an \* in the top, black spectrum are associated with transitions of I<sub>2</sub>(B, v<sub>B</sub>) dissociation products. All of the other features in the two-photon LIF spectrum are attributed to transitions of the Ar···I<sub>2</sub>(B,  $v_B = 23$ , n' = 0) complexes to intermolecular levels bound within the Ar + I<sub>2</sub>(E,  $v_E =$ 0-3) PESs.

Similar LIF spectra were recorded using varying gas mixture concentrations (5%, 10%, and 20% Ar in He), backing pressures (3000–75000 Torr), and distances downstream (5–40 mm). The intensities of all of the Ar···I $_2$  features observed in Fig. 1 scale with each other as the conditions were varied. Consequently, all of these features are attributed to two-color, two-photon transitions of T-shaped Ar···I $_2$ (X,  $v_X=0$ ) complexes to different intermolecular vibrational levels within the Ar + I $_2$ (E,  $v_E=0$ –3) PESs and not to transitions of the linear Ar···I $_2$ (X,  $v_X=0$ ) conformer, higher-order Ar $_n$ ···I $_2$ (X,  $v_X=0$ ) clusters, or He···I $_2$ (X,  $v_X=0$ ) complexes.

The binding energies in the  $Ar + I_2(E, v_E)$  PESs are sufficiently large in comparison to the I<sub>2</sub>(E, v<sub>E</sub>) molecular vibrational spacing, ~100 cm<sup>-</sup> [29], so that the PESs for adjacent v<sub>E</sub> asymptotes are nested within each other. This results in a high density of intermolecular vibrational levels and possible energetic overlap of the spectral features associated with transitions to levels within these different PESs. In order to assign the features associated with each Ar + I2(E, vE) PES, the two-color LIF spectrum shown in Fig. 1 is plotted in Fig. 2 as four different spectra on an energy scale that is relative to each of the four different  $I_2$  E-B,  $v_E$ -23 monomer transition energies with  $v_E = 0$ -3. Since the interactions within the PESs do not change significantly with v<sub>E</sub> for these low vibrational quanta, the two-photon LIF features associated with Ar...I2 transitions that access common intermolecular vibrational levels within the different Ar +  $I_2(E, v_E = 0-3)$  PESs should be observed at nearly the same transition energies relative to the monomer transitions. The features line up well, as shown in Fig. 2, and up to 21 different spectral features spanning a range of 220.9 cm<sup>-1</sup> are assigned, and these are identified as the  $a_{vE}$  through  $u_{vE}$  features for each  $I_2$  E–B,  $v_E$ –23 region. There are no other identifiable Ar···I2 LIF features at energies below the avE feature in each spectral region. Given the appreciable intensities of the a<sub>vE</sub> LIF features, we conclude these features are associated with transitions to the lowest-energy intermolecular vibrational level bound within each of the Ar +  $I_2(E, v_E = 0-3)$  PESs.

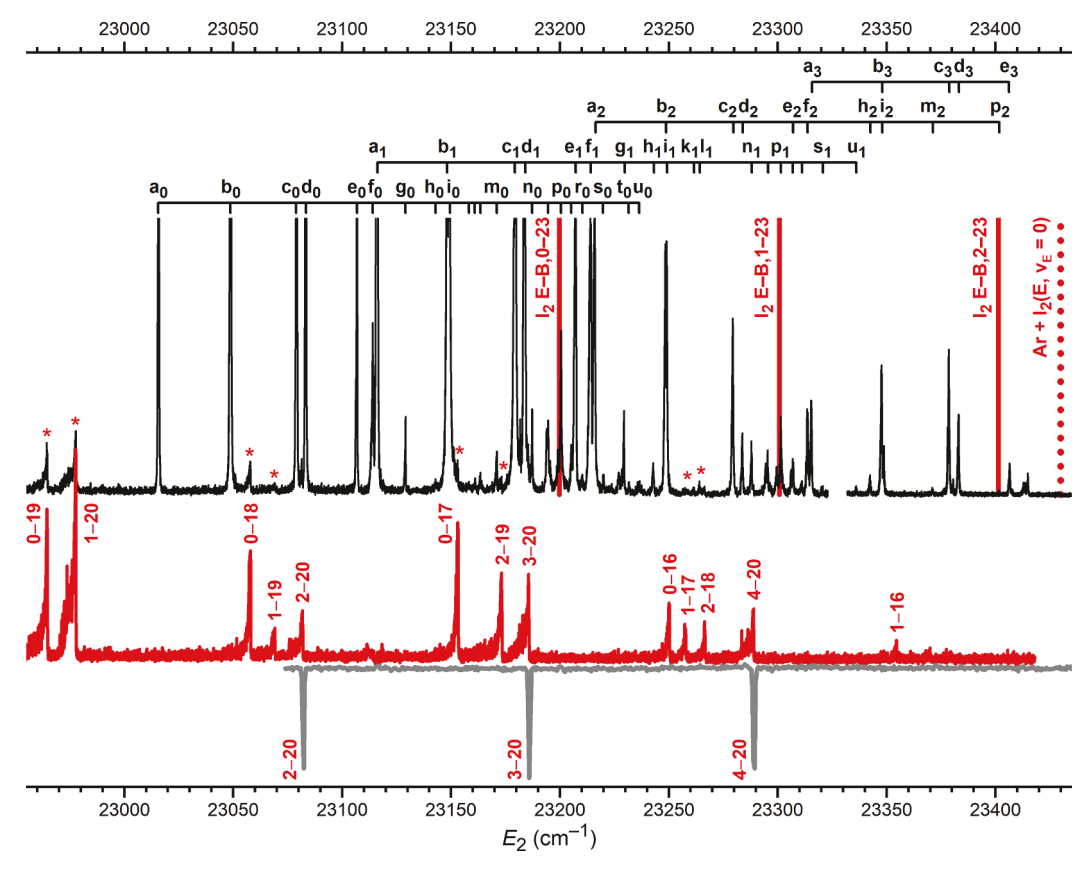


**Fig. 1.** Two-color, two-photon LIF spectra recorded as a function of wavenumber of  $E_2$  through the  $I_2$  E–B,  $v_E$ –23 ( $v_E$  = 0–3) spectral region. The top spectrum (black) was recorded with the  $E_1$  and  $E_2$  pulses overlapped in time and with  $E_1$  = 18169.57 cm<sup>-1</sup>, the transition to the n' = 0, rigidly T-shaped level in the Ar +  $I_2(E, v_B$  = 23) potential. Transitions to the excited-state levels bound within each of the Ar +  $I_2(E, v_E$  = 0–3) potentials are identified with tics and letters representing the ordering of the intermolecular vibrational levels accessed within each potential, denoted by  $v_E$  in the subscript. The  $I_2$  E–B,  $v_E$ –23 transition wavenumbers are indicated with vertical, solid red lines. The Ar +  $I_2(E, v_E$  = 0) dissociation limit is identified with a vertical, dotted red line. Features labeled with an \* are associated with  $I_2$  β–B,  $I_2$  molecular transitions. The middle, red spectrum was recorded in the same manner, but with the  $I_2$  pulses delayed by 20 ns from the  $I_2$  pulses. Features in the red spectrum are  $I_2$  β–B,  $I_2$  transitions, and they are labeled with  $I_2$  β–B,  $I_2$  transitions,  $I_3$  transitions,  $I_4$  and with  $I_2$  delayed by 20 ns from  $I_3$ . The different  $I_3$  β–B,  $I_4$  features are labeled with  $I_4$  fixed on the  $I_2$  B–X, 20–0 monomer transition,  $I_3$  and with  $I_4$  delayed by 20 ns from  $I_4$ . The different  $I_4$  β–B,  $I_4$  features are labeled with  $I_4$  fixed on the  $I_4$  B–X, 20–0 monomer transition,  $I_4$  = 17892.88 cm<sup>-1</sup>, and with  $I_4$  delayed by 20 ns from  $I_4$ . The different  $I_4$  β–B,  $I_4$  features are labeled with  $I_4$  fixed on the  $I_4$  B–X, 20–0 monomer transition.

In order to aid in assigning the LIF spectral features, another two-color, two-photon spectrum was recorded across the same spectral region, but with the excitation laser wavenumber,  $E_1$ , fixed on the transition to the  $\text{Ar} \cdot \cdot \cdot \text{I}_2(\text{B}, \text{ v}_{\text{B}} = 23, \text{ n}' = 2)$  level, 18200.27 cm $^{-1}$  [9]. We assign this n' = 2 level as the " $E_3$  level" calculated by Roncero, et al [6]. The calculated wave function of this level indicates the complex is not rigidly T-shaped, rather the Ar atom is more delocalized along the angular coordinate about the  $E_2$  moiety. The Franck-Condon factors for transitions from this intermolecular vibrational level should result in those spectral features associated with transitions to levels with intermolecular bending excitation or with delocalization of the Ar atom along the angular coordinate having higher intensities relative to those that access levels that are rigidly T-shaped.

Portions of the LIF spectra acquired using the intermediate  $Ar\cdots I_2(B,v_B=23,\,n')$  levels with n'=0 (black) and n'=2 (inverted, gray) are plotted as a function of total excitation energy,  $E_1+E_2$ , in Fig. 3. The intensities of all of the  $Ar\cdots I_2$  features are weaker in the n'=2 spectrum in comparison to those in the n'=0 spectrum due to the notably weaker strength of the transition to the n'=2 level in the  $I_2$  B–X, 23–0 region. While common  $Ar\cdots I_2$  features are observed in both spectra, the relative intensities of these features are distinctly different. The features labeled with  $\dagger$  in the n'=2 spectrum are significantly more intense than the others, and these are correspondingly associated transitions to  $Ar\cdots I_2(E,v_E=0,1)$  levels with intermolecular bending excitation. The relative intensities of the features in the  $I_2$  E–B, 1–23 progression increased relative to those in the 0–23 progression, indicating there is a change in

localization along the angular coordinate induced by the  ${\rm I}_2$  stretching excitation in the E state.

The contrasting intensities of and the energetic spacings between the a<sub>vE</sub> through m<sub>vE</sub> features in the two spectra in Fig. 3 were used to assign the intermolecular bending and stretching excitation of the levels within the Ar +  $I_2(E, v_E = 0,1)$  PESs. The assignments of each of these levels are indicated on the lower tics with  $(n_b,n_s)_{vE}$ , where  $n_b$  and  $n_s$  represent the intermolecular bending and stretching excitation within the Ar + I<sub>2</sub>(E,  $v_{\mbox{\scriptsize E}})$  PES. As already stated, the  $a_{\mbox{\scriptsize vE}}$  transitions access the lowest-energy intermolecular vibrational levels with rigid T-shaped geometries bound within the Ar + I<sub>2</sub>(E,  $v_E$ ) PESs, and they are labeled as  $(0,0)_{vE}$ , or specifically as  $(0,0)_0$  and  $(0,0)_1$  in Fig. 3. The  $b_{vE}$ ,  $c_{vE}$ ,  $e_{vE}$ , and  $g_{vE}$ transitions access the levels with pure intermolecular stretching and no bending excitation, and they are identified as the  $(0,1)_{vE}$ ,  $(0,2)_{vE}$ ,  $(0,3)_{vE}$ , and  $(0,4)_{vE}$  levels. The progressions of features labeled as  $d_{vE}$ ,  $f_{vE}$ ,  $h_{vE}$ , and  $m_{vE}$  are associated with transitions to levels with two quanta of intermolecular bending excitation and increasing stretching excitation,  $(2,n_s)_{vE}$ . These intermolecular vibrational levels must have  $n_b = 2$  and not  $n_b = 1$  due to the  $C_{2v}$  symmetries of the  $Ar + I_2(B, v_B)$  and  $Ar + I_2(E, v_E)$  PESs [6,23]. The  $i_{vE}$  transitions are assigned as accessing the (4,0)<sub>vE</sub> levels, but stretching progressions with this bending excitation are not identified. The spectral assignments, the transition energies, and the energies of the levels below the corresponding Ar + I<sub>2</sub>(E, v<sub>E</sub>) asymptotes are tabulated in Supplementary Materials.

The features corresponding to transitions accessing highly excited intermolecular vibrational levels within the Ar + I<sub>2</sub>(E, v<sub>E</sub>) PESs, >156

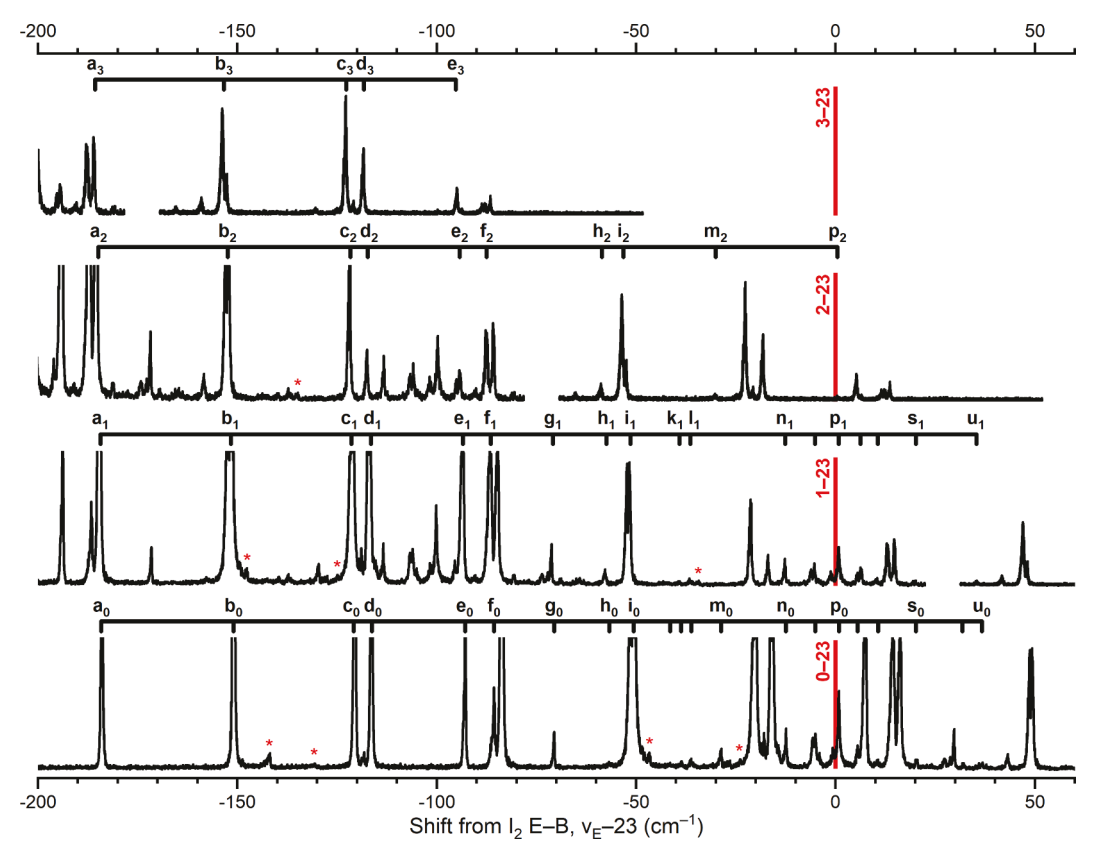


Fig. 2. The two-color, two-photon LIF spectrum included in Fig. 1 with the wavenumber axis representing the shift from the four different  $I_2$  E–B,  $v_E$ –23 transitions, which are labeled and indicated with red vertical lines. Those features associated with transitions to intermolecular vibrational levels within each Ar +  $I_2$ (E,  $v_E$ ) PES are identified with tics and labels. The letters represent the ordering of the observed features, and the subscripts are  $v_E$ . Features labeled with an \* are associated with  $I_2$   $\beta$ –B,  $v_B$ – $v_B$  molecular transitions.

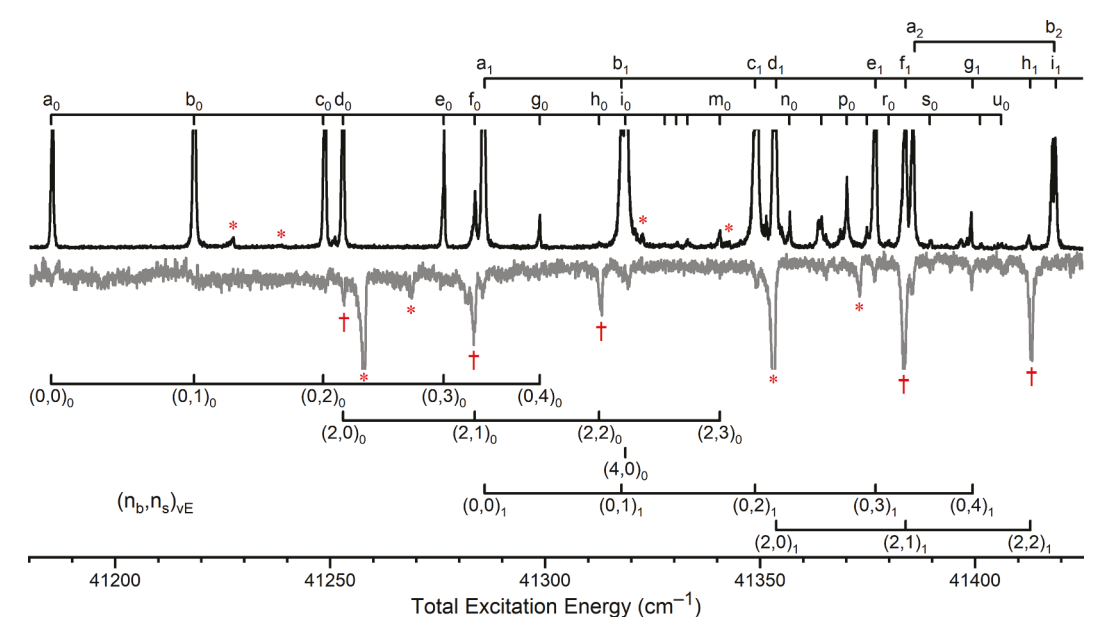


Fig. 3. Two-color, two-photon LIF spectra recorded through the  $I_2$  E-B,  $v_E$ -23 spectral region using different Ar···I $_2$ (B,  $v_B$  = 23, n') intermediate levels. The wavenumber scale is the total excitation wavenumber,  $E_1 + E_2$ , with  $E_1$  fixed and  $E_2$  scanned. The upper, black spectrum is the same as shown in Fig. 1, which was collected using  $E_1$  = 18169.57 cm<sup>-1</sup>, thereby accessing the n' = 0, T-shaped level as the intermediate. The inverted, gray spectrum was acquired using the n' = 2 bending level as the intermediate,  $E_1$  = 18200.27 cm<sup>-1</sup>. The intensities of the Ar···I $_2$  features labeled with a † decreased by a significantly less amount relative to the other features in the gray spectrum, suggesting these transitions access levels with bending excitation. The  $(n_b, n_s)_{vE}$  labels on the lower tics indicate the quanta of intermolecular bending,  $n_b$ , and stretching,  $n_s$ , excitation in the levels accessed within the Ar + I $_2$ (E,  $v_E$ ) PESs. Features labeled with an \* are associated with I $_2$   $\beta$ -B,  $v_{\beta}$ - $v_{\beta}$  molecular transitions.

 ${\rm cm}^{-1}$  above the  ${\rm a}_{\rm vF}$  feature, are congested and do not appear to follow simple energy-spacing patterns. Thus, assignments of those spectral features are not made. The energies of the levels bound within the Ar + $I_2(B, v_B = 20-23)$  PESs also follow simple progressions of intermolecular bending and stretching levels for those low-energy levels accessed by transitions of the T-shaped Ar $\cdots$ I<sub>2</sub>(X, v<sub>X</sub> = 0) complex [9]. In contrast, transitions of the linear  $Ar \cdot \cdot \cdot I_2(X, v_X = 0)$  complex accessed levels that did not have identifiable energy patterns, and this was attributed to these Ar $\cdot\cdot\cdot$ I<sub>2</sub>(B, v<sub>B</sub> = 20–23) levels resembling hindered, internal-rotor states with the Ar atom delocalized about the  $I_2$  molecule [6,9]. These assignments enabled an estimate of 90-110 cm<sup>-1</sup> for the energetic barrier from the lowest-energy T-shaped level, which has a binding energy of  $\sim 227~\text{cm}^{-1}\text{,}$  to rotation of the Ar atom about the  $I_2$  molecule within the Ar + I<sub>2</sub>(B,  $v_B$  = 20–23) PESs to be made. This energetic barrier represents 40-50% of the well depth. In a similar manner, the highestenergy intermolecular level assigned in the Ar + I<sub>2</sub>(E,  $v_E = 0$ –2) PESs that seems to be largely localized within the T-shaped well is the (2,3)v<sub>E</sub> level. The  $(2,3)_0$  level lies 155.5 cm<sup>-1</sup> above the  $(0,0)_0$  level, which is bound by  $\sim 410~{\rm cm}^{-1}$ , as will be described below. The barrier to rotation of the Ar atom about the  $I_2$  within the Ar +  $I_2(E, v_E = 0-2)$  PESs is then estimated to be  $\sim 165 \text{ cm}^{-1}$ , which is just below where the transition to the  $(4,1)_0$  level is expected to be. This barrier to rotation represents 40% of the well depth.

The assignments of the lower-lying levels enable harmonic vibrational frequencies and anharmonic vibrational constants for the intermolecular stretching modes in the  $Ar + I_2(E, v_E)$  PESs to be determined. The energies of the  $(0,n_s)_{vE}$  intermolecular stretching levels below the corresponding asymptote were plotted as a function of stretching excitation,  $n_s$ , and fit to a simple anharmonic progression,  $E(n_s) = \omega_e(s)(n_s +$  $\frac{1}{2}$ ) –  $\omega_e \chi_e(s) (n_s + \frac{1}{2})^2$ . The fits are included in Supplementary Materials. The intermolecular vibrational stretching frequency and anharmonic constant obtained in the fitting of the stretching levels bound within the Ar +  $I_2(E, v_E = 0)$  PES are  $\omega_e(s) = 37.1(1.0)$  cm<sup>-1</sup> and  $\omega_e \chi_e(s) = 1.7(2)$ cm<sup>-1</sup>, and the stretching frequencies for the other v<sub>E</sub> PESs are included in Table 1. These stretching frequencies are the same within error to those reported by Baturo, et al [19,20]. The identification of intermolecular bending levels, not assigned previously, enabled estimates of the vibrational frequencies and anharmonic constants for the intermolecular bending motion to be made. These fits are included in Supplementary Materials, and the values for the Ar +  $I_2(E, v_E=0)$  PES are  $\omega_e(b)\sim 34.8~cm^{-1}$  and  $\omega_e\chi_e(b)\sim 0.3~cm^{-1}.$  The bending frequencies for the other v<sub>E</sub> PESs are included in Table 1. The vibrational frequencies of the T-shaped levels within the Ar + (B,  $v_B = 21$ ) [9], He + I<sub>2</sub>(E,  $v_E = 1$ ) [25], He + ICl(E,  $v_E = 11$ ) and He + ICl( $\beta$ ,  $v_{\beta} = 1$ ) [26] PESs are also given in Table 1 for comparison. Intermolecular vibrational frequencies for the He + I<sub>2</sub>(B,  $v_B = 21$ ) and He + ICl(B,  $v_B = 3$ ) PESs could not be

**Table 1** Binding energies,  $D_0$ , harmonic bending,  $\omega_e(b)$ , and stretching,  $\omega_e(s)$ , frequencies in units of cm $^{-1}$  for several T-shaped rare gas···dihalogen complexes in the indicated states.

		Ref	$D_0$	ω <sub>e</sub> (b)	$\omega_{\rm e}(s)$
$Ar \cdots I_2$	$X, v_X = 0$	[9,16]	240.5		
	B, $v_B = 21$	[9]	226.8	~15.4	~28
	$E,v_E=0$		410.3	~34.8	37.1
	E, $v_E = 1$		410.9	~34.9	36.5
	$E,v_E=2$		411.8	~35.1	35.4
He…I <sub>2</sub>	$X, v_X = 0$	[25]	16.6		
	B, $v_{B} = 21$	[25]	12.8		
	$E,v_E=1$	[25]	16.7	~3.2	~2.6
He···ICl	$X, v_X = 0$	[26]	16.6		
	B, $v_B = 3$	[26]	13.3		
	E, $v_E = 11$	[26]	40.3	12.1	25.7
	$\beta\text{, }v_{\beta}=1$	[26]	41	14.7	27.9

determined since only the first two intermolecular levels are bound in the T-shaped well, and all other bound levels are delocalized and referred to as free-rotor states [25,31].

The binding energies of the  $Ar \cdots I_2$  complexes in the  $Ar + I_2(E, v_E = 0-3)$  PESs were determined as illustrated in Fig. 4 for the  $v_E = 0$  potential. Following this diagram, the sum of the energies indicated by the red arrows equals the sum of the energies of blue arrows.

$$E_1(Ar\cdots I_2) + E_2(Ar\cdots I_2) + D_0(E) = D_0(X) + E_1(I_2) + E_2(I_2)$$

The two-photon, total excitation energy to the  $(0,0)_0$  lowest-energy level is  $E_1(Ar\cdots I_2)+E_2(Ar\cdots I_2)=41185.4(1)$  cm $^{-1}$ . The sum of the  $I_2$  B–X, 23–0 and  $I_2$  E–B, 0–23 transition wavenumbers is  $E_1(I_2)+E_2(I_2)=41355.2(1)$  cm $^{-1}$ . The binding energy of the T-shaped Ar··· $I_2(X, v_X=0)$  conformer,  $D_0(X)$ , was measured to be 240.5(3.6) cm $^{-1}$  [9,16]. These values yield a binding energy of  $D_0(E)=410.3(3.6)$  cm $^{-1}$  for the Ar +  $I_2(E, v_E=0)$  PES. The binding energies within the Ar +  $I_2(E, v_E=1-3)$  PESs were obtained in a similar manner,  $D_0(E)=410.9(3.6)$ , 411.8(3.6) and 412.5(3.6) cm $^{-1}$ , respectively. These binding energies are the same within error as those reported by Baturo, et al [20], and they are compared with those of the He···I2 and He···ICl complexes in Table 1.

#### 4. Conclusions

Two-color, two-photon LIF experiments were performed to characterize the intermolecular vibrational levels bound within the Ar + I<sub>2</sub>(E,  $v_E = 0$ –3) PESs. Assignments of many of the observed Ar $\cdots$ I<sub>2</sub> LIF features were made by recording spectra using different intermolecular vibrational levels within the Ar +  $I_2(B, v_B = 23)$  PES as the intermediates to contrast the Franck-Condon overlaps and relative intensities of the transitions [9]. The stretching frequencies in the ion-pair state potentials are the same within error to those reported by Baturo, et al [19,20]. The intermolecular bending features were not previously reported, and the intermolecular bending vibrational frequency and anharmonic constant were determined to be  $\omega_e(b)\sim 34.8~\text{cm}^{-1}$  and  $\omega_e\chi_e(b)\sim 0.3~\text{cm}^{-1}.$  As quantitative details describing the intermolecular interactions of rare gas atoms and iodine in the ion-pair states are currently lacking, a few observations regarding the data in Table 1 that may provide targets for calculations are highlighted. The binding energy of the  $Ar + I_2(E, v_E = 0)$ PES, ~410 cm<sup>-1</sup>, is 80% larger and the harmonic intermolecular bending frequency, 34.8 cm<sup>-1</sup>, is more than two times larger than the values reported for the Ar +  $I_2(B, v_B = 21)$  PES [9]. The intermolecular bending and stretching frequencies are nearly the same in the Ar +  $I_2(E,$ v<sub>E</sub> = 0) PES, but the stretching frequency is 80% larger than bending

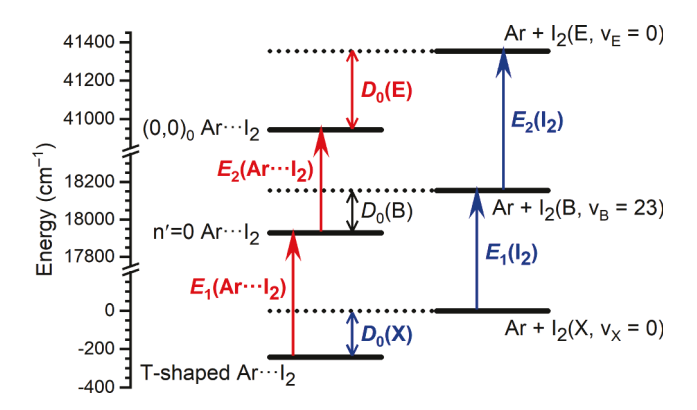


**Fig. 4.** Schematic energy-level diagram indicating the excitation of the T-shaped Ar···I<sub>2</sub> complexes and I<sub>2</sub> molecules in the two-photon LIF spectra. The I<sub>2</sub> B–X, 23–0 and I<sub>2</sub> E–B, 0–23 transition energies are indicated by red arrows and labeled as  $E_1(I_2)$  and  $E_2(I_2)$ , respectively. The transition energies of the Ar···I<sub>2</sub> complex to the n'=0 level and the  $(0,0)_0$  level are also indicated by red arrows and are labeled as  $E_1(Ar···I_2)$  and  $E_2(Ar···I_2)$ , respectively. The binding energies of the in the Ar + I<sub>2</sub>(X, v<sub>X</sub> = 0), Ar + I<sub>2</sub>(B, v<sub>B</sub> = 23), and Ar + I<sub>2</sub>(E, v<sub>E</sub> = 0) PESs are labeled as  $D_0(X)$ ,  $D_0(B)$ , and  $D_0(E)$ .

frequency in the Ar +  $I_2(B, v_B=21)$  PES. We attribute these differences to the contrasting anisotropies of these PESs. The interactions of the less-polarizable He atom with  $I_2$  result in nearly identical binding energies for the T-shaped level in the He +  $I_2(X, v_X=0)$  PES and the He +  $I_2(E, v_E=1)$  PES, and an  $\sim$  25% smaller binding energy in the He +  $I_2(B, v_B=21)$  PES. The experimentally determined binding energies of the Ar +  $I_2(E, v_E)$  and He +  $I_2(E, v_E)$  PESs are not consistent with the well depths of the potentials calculated using several variants [24].

## CRediT authorship contribution statement

**Camille Makarem:** Conceptualization, Methodology, and original draft preparation, performed the experiments. **Richard A. Loomis:** Conceptualization, Methodology, Writing – original draft, edited and prepared the final manuscript.

# **Declaration of Competing Interest**

The authors declare the following financial interests/personal relationships which may be considered as potential competing interests: Richard A. Loomis reports financial support was provided by National Science Foundation. Richard A. Loomis reports financial support was provided by American Chemical Society Petroleum Research Fund.

#### Data availability

Data will be made available on request.

#### Acknowledgements

This work was partially supported by the NSF under grant CSDMA-2102241. Acknowledgment is made to the donors of the American Chemical Society Petroleum Research Fund for partial support of this research.

### Appendix A. Supplementary data

Supplementary data to this article can be found online at https://doi.org/10.1016/j.cplett.2023.140642.

#### References

- [1] A. Rohrbacher, J. Williams, K.C. Janda, Phys. Chem. Chem. Phys. 1 (1999) 5263.
- [2] A. Rohrbacher, N. Halberstadt, K.C. Janda, Ann. Rev. Phys. Chem. 51 (2000) 405.
- [3] A. Buchachenko, N. Halberstadt, B. Lepetit, O. Roncero, Int. Rev. Phys. Chem. 22 (2003) 153.
- [4] C. Makarem, J. Wei, R.A. Loomis, J.P. Darr, Phys. Chem. Chem. Phys. 23 (2021) 26108.
- [5] J.A. Blazy, B.M. DeKoven, T.D. Russell, D.H. Levy, J. Chem. Phys. 72 (1980) 2439.
- [6] O. Roncero, B. Lepetit, J.A. Beswick, N. Halberstadt, A.A. Buchachenko, J. Chem. Phys. 115 (2001) 6961.
- [7] A.A. Buchachenko, O. Roncero, N.F. Stepanov, Russ. J. Phys. Chem. 74 (2000) S193.
- [8] B. Kubiak, P.S.H. Fitch, L. Wharton, D.H. Levy, J. Chem. Phys. 68 (1978) 4477.
- [9] C. Makarem, R.A. Loomis, Chem. Phys. Lett. 651 (2016) 119.
- [10] M.L. Burke, W. Klemperer, J. Chem. Phys. 98 (1993) 6642.
- [11] M.L. Burke, W. Klemperer, J. Chem. Phys. 98 (1993) 1797.
- [12] J.P. Darr, J.J. Glennon, R.A. Loomis, J. Chem. Phys. 122 (2005), 131101.
- [13] A. Burroughs, M.C. Heaven, J. Chem. Phys. 114 (2001) 7027.
- [14] F.Y. Naumkin, ChemPhysChem 2 (2001) 121.
- [15] R. Prosmiti, P. Villarreal, G. Delgado-Barrio, Chem. Phys. Lett. 359 (2002) 473.
- [16] J. Wei, C. Makarem, A.L. Reinitz, J.P. Darr, R.A. Loomis, Chem. Phys. 399 (2012)
- [17] A.A. Buchachenko, N.F. Stepanov, J. Chem. Phys. 104 (1996) 9913.
- [18] F.Y. Naumkin, Chem. Phys. 226 (1998) 319.
- [19] V.V. Baturo, I.N. Cherepanov, S.S. Lukashov, S.A. Poretsky, A.M. Pravilov, Chem. Phys. Lett. 647 (2016) 161.
- [20] V.V. Baturo, S.S. Lukashov, S.A. Poretsky, A.M. Pravilov, Eur. Phys. J. D 71 (2017) 227.
- [21] M.E. Akopyan, S.S. Lukashov, S.A. Poretsky, A.M. Pravilov, Russ. J. Phys. Chem. 83 (2009) 116.
- [22] S.S. Lukashov, I.Y. Novikova, S.A. Poretsky, A.M. Pravilov, A.S. Torgashkova, Chem. Phys. 336 (2007) 109.
- [23] T.V. Shcherbul', A.V. Zaitsevskii, A.A. Buchachenko, N.F. Stepanov, Russ. J. Phys. Chem. 77 (2003) 511.
- [24] T.V. Shcherbul', Y.V. Suleimanov, A.A. Buchachenko, Russ. J. Phys. Chem. 80 (2006) 1957.
- [25] S.E. Ray, A.B. McCoy, J.J. Glennon, J.P. Darr, E.J. Fesser, J.R. Lancaster, R. A. Loomis, J. Chem. Phys. 125 (2006), 164314.
- [26] J.P. Darr, R.A. Loomis, J. Chem. Phys. 129 (2008), 144306.
- [27] N. Zeigler, C. Makarem, J. Wei, R.A. Loomis, J. Chem. Phys. 152 (2020), 094303.
- [28] K.E. Johnson, W. Sharfin, D.H. Levy, J. Chem. Phys. 74 (1981) 163.
- [29] J.C.D. Brand, A.R. Hoy, A.K. Kalkar, A.B. Yamashita, J. Mol. Spectrosc. 95 (1982) 350.
- [30] J.P. Perrot, M. Broyer, J. Chevaleyre, B. Femelat, J. Mol. Spectrosc. 98 (1983) 161.
- [31] A.B. McCoy, J.P. Darr, D.S. Boucher, P.R. Winter, M.D. Bradke, R.A. Loomis, J. Chem. Phys. 120 (2004) 2677.